Image Cover Sheet

CLASSIFICATION	SYSTEM NUMBER
UNCLASSIFIED	60722

TITLE

EXPERIMENTAL DETERMINATION OF INTERFRAME BUCKLING OF A RING STIFFENED CYLINDER

System Number:

Patron Number:

Requester:

Notes:

DSIS Use only:

Deliver to: JR

UNLIMITED DISTRIBUTION

National Defence
Research and Development Branch

Défense nationale
Bureau de recherche et développement

EXPERIMENTAL DETERMINATION OF INTERFRAME BUCKLING OF A RING STIFFENED CYLINDER

N.G. PEGG

May 1989

Approved by L.J. Leggat
Director/Technical Division

Distribution Approved by

D/TD

TECHNICAL MEMORANDUM 89/209

Defence Research Establishment Atlantic

Centre de Recherches pour la Défense Atlantique

Canada

Abstract

An experimental determination of the interframe buckling collapse of a ring stiffened cylinder subjected to hydrostatic pressure is presented. This test served two purposes, the first to experimentally verify finite element predictions of the buckling collapse behaviour, the second to evaluate the possibilities of using an existing high pressure facility for conducting model tests of more complex pressure vessel models. The finite element and experimental results for the collapse load and mode were in good agreement. A method of determining the elastic buckling collapse load by measuring the decreasing frequencies of vibration modes corresponding to buckling collapse modes has also been investigated with encouraging results. The high pressure tank served the purpose of conducting the experiment, although the inability to physically observe the test did cause some difficulties in determining the actual collapse load.

Résumé

L'étude expérimentale porte sur le flambage entre bâtis d'un cylindre renforcé de raidisseurs circulaires et soumis à une pression hydrostatique. L'essai avait pour objet : 1° de vérifier l'exactitude des prévisions de conditions de flambage, calculées d'après la méthode des éléments finis, et 2° d'évaluer les avantages de l'utilisation d'un installation d'essai à haute pression existant pour des essais sur modèle de composants d'appareils soumis à pression plus complexes. Les résultats de l'expérience et ceux des calculs par la méthode des éléments finis concordaient, tant pour le mode que pour la charge de flambage. Une autre méthode, visant à déterminer la charge de flambage élastique par la mesure des fréquences décroissantes des modes vibratoires correspondant au modes de flambage, a également reçu évaluation favorable. Le réservoir de haute pression a bien joué son rôle dans l'expérience, bien que la nature éloignée de l'essai rende difficile la mesure de la charge de flambage.

Contents

Notation

a	shell radius to mid thickness
A	$\frac{a^2 A_f}{\overline{d}^2}$
A_f	area of ring stiffener
b	faying flange width
$\overline{d}$	distance from cylinder axis to frame centroid
E	Young's modulus
h	shell wall thickness
L	length of shell bay between stiffeners
n	circumferential harmonic wave number
P_{cr}	critical interframe buckling pressure
P_c	pressure at which outer shell surface at midbay reaches yield
P_s	pressure at which inner shell surface at stiffener reaches yield
σ_y	yield stress
ν	Poisson's ratio
ρ_w	density of water
γ	$\frac{A(1-\frac{\nu}{2})}{A+bh+\frac{2Lh\eta}{\alpha}}$
$\overline{H}$	$-2\frac{\{[1+sqrt\frac{3\nu^2}{1-\nu^2}]\sinh\frac{\alpha}{2}\cos\frac{\alpha}{2}+[1-\sqrt{\frac{3\nu^2}{1-\nu^2}}\cosh\frac{\alpha}{2}\sin\frac{\alpha}{2}]\}}{\sinh\alpha+\sin\alpha}$
$\overline{R}$	$\frac{\sinh\alpha-\sin\alpha}{\sinh\alpha+\sin\alpha}$
α^4	$\frac{3L^4(1-\nu^2)}{a^2h^2}$
η	$\frac{\cosh\alpha-\cos\alpha}{\sinh\alpha+\sin\alpha}$

1 Introduction

The prediction of collapse loads for externally pressurized vessels is complicated by the uncertain effects of shape imperfections, material nonlinearities and asymmetric structure and/or load. Typically, designs are based on predictions of the linear elastic bifurcation buckling loads of 'perfect' structure, together with application of 'knockdown factors' to account for the possible effects of geometric, material or load uncertainties. In lieu of the use of knockdown factors, detailed finite element analyses may, in principle, be used to take explicit account of imperfections, nonlinearities, and complex structure and load functions.

Detailed finite element analyses of submarine pressure vessel structure are being studied at the Defence Research Establishment Atlantic (DREA). This memo describes an experiment to provide the necessary verification of finite element interframe buckling collapse predictions of a ring stiffened cylinder and to evaluate a high pressure tank facility for conducting model tests.

DREA has a high pressure water tank for proof testing equipment intended for use in deep ocean conditions. To evaluate this facility for conducting pressure vessel model tests, a machined aluminum ring stiffened cylinder designed to fail in an elastic interframe buckling mode, was tested to failure. The model was machined from aluminum tubing to obtain as perfect a structure as possible and then measured to obtain the variations in shell thickness and radius. The shell material was also tested to obtain Young's modulus and yield stress values. Strain gauges were placed at several locations on the model, providing the only means of monitoring its behaviour during the tests. The strain gauge information was used to detect the failure point directly through observing sudden changes in strain, and indirectly through determining the change in vibration frequencies with increasing pressure. These test data were also compared to results from an axisymmetric finite element analysis carried out with the linear elastic code VAST[1] developed by DREA.

Section 2 of this memorandum briefly describes the basic theory of buckling and collapse of ring stiffened pressure vessels. The theory of using vibration modal information to nondestructively determine buckling pressure is also discussed. Section 3 describes the test model followed by a discussion of the finite element model of the cylinder in Section 4. The pressure tank facility and test procedure are described in Section 5 and the experimental and numerical stress and collapse results are given in Section 6.

2 Background Theory

A ring stiffened cylinder under hydrostatic pressure (such as the model investigated here and shown in Figure 1) can fail through buckling or yielding. Buckling failure may occur in the elastic material phase of behaviour or after the material has started to yield. The critical buckling mode for ring stiffened cylinders occurs in one of two forms. One is overall instability (Figure 2) which usually occurs in a mode with 2 to 4 waves circumferentially and a half wave between rigid ends. The other form is interframe instability (Figure 3) which occurs in a mode with a higher number of circumferential waves (6 to 20) and half waves between ring stiffeners. In this particular study interframe buckling failure was investigated. The critical points for yielding failure, shown in Figure 4, are: the circumferential stress at the outer surface of the shell at midbay between stiffeners; and, the axial stress at the inner surface of the shell at the shell-stiffener connection. Strain gauges were placed on the model to monitor these locations.

The test procedure was, basically, to increase the pressure in the tank and observe the strain gauge and pressure transducer responses for occurrence of buckling or yielding.

Another method of determining instability experimentally is to observe the values of the vibration frequencies which correspond to buckling mode shapes. For uniform models under uniform loading, the mode shapes for vibration and buckling will be similar. It is well known that as the stiffness of a structure is reduced, its natural frequency of vibration drops as the square root of the stiffness (ie. frequency $\propto \sqrt{\frac{k}{m}}$). As the structure approaches its buckling load, its stiffness approaches zero and hence so does its natural frequency of vibration. This is easily understood for a simple structure such as a column under an increasing axial load where the principle buckling and vibration modes are well known. For the ring stiffened cylinder, this is more complex, as there are several buckling and vibration modes which may be the principle mode of buckling failure. For axisymmetric cylinders, the modes of buckling and vibration are separated into circumferential harmonics, there being an infinite number of circumferential harmonics each with an infinite number of eigenmodes describing the longitudinal variation of the mode shape. We are concerned with only the first eigenmodes of each circumferential harmonics since they produce the lowest buckling load for each harmonic. Therefore, in considering the lowest buckling mode for each circumferential harmonic, there is an associated vibration mode whose frequency approaches zero as the buckling load for that mode is reached. Of course, only the frequency of one of the harmonics will reach zero, that corresponding to the lowest (critical) buckling mode. The frequencies decrease as the square root of the applied load since the stiffness terms for each harmonic are directly proportional to the applied load. By using measured vibration data from the model as the pressure is increased, the critical buckling load can be determined by extrapolating the data to zero frequency. This technique has been used by Singer[2] for axially loaded cylinders. He also proves that this technique includes the effects of imperfections and uncertain boundary conditions in determining the actual buckling load of the structure. In this present study this method is considered only as a secondary investigation,

as the cylinder strain gauge monitoring did not provide enough data to distinguish the higher order mode shapes of interframe vibration. Correlating the experimentally determined vibration frequencies (from the strain gauge data) with finite element predictions of the vibration frequencies, at increasing pressure, allowed a means to identify possible modes, and did give some useful results.

Experimental determination of buckling loads is certainly not a new field, and there have been many studies to investigate buckling loads for a variety of pressure vessel geometries and loads (reference 3 for example). It has been recognized in past studies that careful geometric measurement of the model is essential in interpreting test results. Measurements were also made in this study, but since the model was, in fact, machined very near to the ideal geometry, imperfections were not a significant factor in the model failure.

3 Test Model

The test model was designed to be as close to a perfect structure as possible and to fail in an elastic interframe buckling mode so that the VAST linear, elastic finite element model would represent its behaviour. The ring stiffened model was created by machining a section of 8x0.5 inch aluminum tubing. The dimensions of the model are shown in Figure 5, and a photograph of the model in Figure 1.

The material was chosen from shop stock and its exact type was unknown, although it was believed to be aluminum 6061-T6. Uniaxial tension and compression tests were conducted to determine Young's modulus and yield stress. An example of one of the compression tests is shown in Figure 6. A value of Young's modulus of 10,000,000 psi, in agreement with the usual published values for aluminum, was derived from all tests. The yield stress varied marginally from 40,340 to 41,182 psi at 0.002 strain over six tests. A value of 41,000 psi, commonly used for 6061-T6, was used as the yield stress in this study.

The model was manufactured by The Ship Repair Unit (Atlantic) of Maritime Command. First, a thin layer was machined off the inside to ensure circularity, and then material was machined off external sections to create the ring stiffeners. Dial gauge measurements of inner and outer radii were made at each ring, and at midbay between each ring, at eight circumferential locations. Figure 7 shows the variation in the radii to the outside of the ring stiffeners along the length of the shell. There are 8 angular locations, where the symbol 1 is at 0 degrees, 2 at 45 degrees, 3 at 90 degrees, etc. The variation (difference between minimum and maximum), excluding the low value at the cylinder end, is 0.038 inches over a nominal radius of 4.0 inches.

Figure 8 shows the same type of graph as Figure 7 for the outside shell radii at midbay. The variation is 0.011 inches over a nominal value of mean (midthickness) radius of 3.548 inches (the value used in the finite element model). Figure 9 shows the inside shell radii with a variation of 0.0068 inches. Figure 10 shows the shell thickness with a variation of 0.01 inches over a nominal design value of 0.06 inches. From these data, the maximum out of circularity, determined as the maximum deviation from the mean radius, is 0.14 percent of the mean radius, which is well below recommended design values of 0.5 percent[4].

The variations in the inner and outer radii versus circumferential angle were also determined. Figure 11 shows this for the center bay (where failure occured). A single sine wave is evident indicating that the measurement system may be misaligned or that the model may have a slight overall bend. The thickness is given by the difference between the two lines which is seen to vary slightly around the model. In retrospect, more circumferential locations should have been used to assess imperfections in higher circumferential harmonics.

Figure 5 also shows the strain gauge locations on the inside of the shell wall. Both axial and circumferential strain directions were measured at positions at midbay between stiffeners and at the edge of the stiffener-shell connection. The gauges were Micro-Measurement uniaxial and biaxial EA-06-125TM-120. Two gauges were also placed at midbay in the circumferential

direction on the outside of the shell.

The model was fitted with heavy endcaps to act as rigid ends. A solid aluminum core, with diameter one inch less than the inner diameter of the model was loosely fitted on the rigid ends to act as a stop mechanism when the model collapsed. The core, which was included to avoid possible shock damage to the pressure tank pump when collapse occurred, did not affect the results.

4 Analytical Model

The analytical results were determined by closed form solution and numerical finite element analysis. The closed form solution for the interframe buckling load is that of Von Mises modified by Kendrick[5]:

$$P_{cr} = \frac{Eh}{a(n^2 - 1 + \frac{\pi^2 a^2}{2L^2})}\left[\frac{1}{[n^2(\frac{L}{\pi a})^2 + 1]^2} + \frac{h^2}{12a^2(1-\nu^2)}[n^2 - 1 + (\frac{\pi a}{L})^2]\right] \quad (1)$$

applied to a single bay between frames. This formula has to be used for several values of the circumferential harmonic, n, to acheive the minimum value of the buckling load. The closed form solutions for the pressure values to cause yield are[6or7]:

$$P_C = \frac{h\sigma_y}{a}(\frac{1}{1+\gamma\overline{H}}) \quad (2)$$

for the circumferential stress at the midbay outer fiber and:

$$P_S = \frac{2h\sigma_y}{a}(\frac{1}{[1+(\frac{12}{1-\nu^2})^{\frac{1}{2}}]\gamma\overline{R}}) \quad (3)$$

for the meridional (axial) stress at the inner surface at the shell-stiffener connection (see Figure 4).

The elastic interframe buckling load and stress values were also determined by finite element methods with VAST. Axisymmetric, three node shell elements were used to model the ring stiffened shell (Figure 12). One shell element was used for each stiffener and 8 elements were used between stiffeners. Hydrostatic pressure was applied to the model with an equivalent concentrated end load to represent the pressure on the ends. The asymmetric buckling loads and vibration frequencies are determined by formulating stiffness matrices for each circumferential harmonic and solving the eigenvalue problem for each harmonic[8]. The buckling eigenvalues are determined by solving for the roots of the linear and geometric stiffness equation:

$$[[K] + \lambda([K_G] + [K_F])]_n = 0 \quad (4)$$

where λ_n are the buckling eigenvalues directly proportional to the applied load, $[K]_n$ is the linear stiffness matrix for circumferential harmonic, n, and $[K_G]_n$ is the geometric harmonic stiffness matrix. $[K_F]_n$ is the linearized follower force or load stiffness matrix which accounts for the nonlinear effect of the pressure vectors remaining normal to the shell surface during deformation. The frequency eigenvalues are determined by solving the similar problem for the stiffness and mass matrix:

$$[[K] + \lambda[M]]_n = 0 \quad (5)$$

where $[M]_n$ is the mass matrix and λ_n are the frequency eigenvalues. In determining the vibration frequencies of the model including the effects of an applied hydrostatic pressure, the eigenvalue problem becomes:

$$[([K] + [K_G]) + \lambda[M]]_n = 0 \tag{6}$$

where $[K_G]_n$ incorporates the effects of the applied prestress and $([K] + [K_G])_n$ is the total stiffness which reduces towards zero as the applied compressive pressure is increased.

The pressure tank uses water as its pressurizing medium so the added fluid mass associated with the cylinder motion is required in the mass matrix to determine the vibration frequencies of the model in the tank. At present there are no axisymmetric fluid elements in VAST which can be used in the harmonic, asymmetric mode shape determination (fluid elements for the axisymmetric, n=0, mode exist). Therefore, the added mass for rigid body motion of a cylinder ($= \rho_w \pi a^2 L$) was determined and modelled as an equivalent density added to the shell wall material. This approximation should be very good for the lower harmonics (n=0,1,2 and 3), but may lose some accuracy for higher harmonics; however, it was the only method available aside from developing three dimensional models, which would have been prohibitively large for accurate modelling of the higher order harmonic modes.

5 Test Procedure

The pressure tank is illustrated in Figure 13. It has mainly been used to proof test equipment intended for use in deep ocean conditions to a maximum pressure of 8500 psi. The chamber lid is fitted with a breach lock. Fittings for external monitoring are located in the bottom and top of the chamber. Pressure is increased by pumping water into the chamber. There is no control over the rate of pressure increase. Starting and stopping the pump was the only way to control the tank pressure. Since pressure increased fairly rapidly, and since time was required to inspect the strain gauges and also to collect enough data samples at each load level to determine vibration frequencies, the load was increased in increments of 50 psi (by starting and stopping the pump) until failure. The pump also excited small shock waves in the fluid, even while it idled. This served as the necessary excitation function to excite vibration modes in the model. This characteristic of the apparatus was not known prior to the experiment, but significant vibrations (measurable from strain gauge data) occured, which spurred the secondary investigation into the decreasing frequency method.

The model was suspended vertically from a frame (Figure 13) to minimize the strains resulting from self weight and buoyancy. Strains were measured in this position and found to be negligible. A pressure transducer with a maximum output of 1000 psi was used to measure the applied pressure.

Strain gauge and pressure data were recorded on analogue tape. Chart recorders were used to inspect the data visually as the test progressed. A drop in pressure or nonlinearities in the strain data were expected as the model buckled. Some nonlinearity was detected in a gauge on the buckled bay but this was only just before the model imploded, which was detectable on all of the instrumention, and audibly.

The vibration frequencies were determined by using a spectrum analyzer on the circumferential strain gauge in the buckled bay. Frequency spectra were generated for several load levels.

6 Results and Discussion

The test model failed catastrophically with no prior detectable indication of collapse. At collapse, the model formed its buckled shape, and the shell completely tore away from the heavy ring stiffener. From the stress and pressure data prior to and during the collapse, shown in Table 1, the experimental collapse load appeared to be 587 psi. Figures 14 and 15 show the collapsed model. From Figure 14 it can be seen that the model failed in the center bay (bay 5, see Figure 5) with buckling failure also evident in bay 4. Figure 15 shows the failed cross section where 9 circumferential waves are quite evident. The model collapsed onto the central core in the model, hence the flattened waves. This is quite clearly an interframe failure in mode 9. The actual elastic buckling load is probably a little less than 587 psi as the buckles should have formed before complete yielding collapse, although this could not be detected in the strain gauge data. Prior to collapse, pressure was held steady at about 540 psi for about 40 seconds and then increased towards 590 psi where collapse occured just as the pump was being turned off. The pressure data in the failure region are shown in Figure 16. It can be concluded from this data that the elastic buckling collapse occurred somewhere between 540 and 587 psi.

The Von Mises-Kendricks formula (equation 1) predicted an elastic interframe buckling load of 556 psi in circumferential harmonic n=8. Since this formula assumes a section of shell simply supported between rigid rings, it should predict conservative values for a continuous ring stiffened cylinder.

The VAST model shown in Figure 12 predicted a minimum buckling load of 568 psi in circumferential harmonic n=8. This was closely followed by a buckling load of 588 psi in harmonic n=9. Figure 17 shows the first two eigenvalues for each of the first 10 circumferential harmonics from the VAST analysis. This is a typical graph for ring stiffened pressure vessels such as submarine hulls, with two minima; one for the overall buckling load (in this case at n=2) and one for the interframe buckling load (in this case at n=8). Figures 18 and 19 show the VAST model mode shapes corresponding to the n=8 and n=9 buckling harmonics respectively. Note that the mode for harmonic 9 (Figure 19) is very similar to the experimental mode shape (Figures 14 and 15). This is expanded into a three dimensional form in Figure 20 for better comparison to the experimental shape. Since this is a uniformly stiffened cylinder, it is quite natural to have several interframe modes with almost the same buckling load, and the one in which it actually fails is difficult to predict. Hence, the fact that it failed in harmonic n=9 instead of the predicted n=8 is neither unexpected nor significant.

The strain gauge data were converted to stress for some of the gauges. The midbay circumferential and meridional stress for the inner surface of bay 3 and the midbay circumferential stress at the inner and outer surface of bay 4 are given in Table 2 for a section of the test in the range of 350 psi pressure. Table 1, which was already briefly mentioned, gives the meridianal stress on the inner shell surface and the midbay circumferential and meridianal stress on the inner shell surface of bay 5 (where failure occurred) for the test in the failure range. Figure

21 shows the stress values for the last 80 seconds of the test corresponding to Table 1. Figure 16 showed the pressure data for the same period. The influence of the pressure loading steps can be seen in the figures. As can be seen, the data were certainly not smooth. Some of the probable causes of this were: 60 Hz line noise which was very evident in the frequency analysis of the data (to be discussed later), pressure fluctuations in the tank from the pump vibration, and excitation of vibration modes in the test model. It was not expected that the data would fluctuate so much; this will have to be investigated further in subsequent tests.

In looking at the measured midbay stresses in Tables 1 and 2, it can be seen that the meridional values are about half the circumferential values, as would be expected. There is very little difference between the inner and outer surface circumferental stress indicating pure membrane behaviour at midbay, and also little difference between bays in the central part of the model. These too, are expected results.

Agreement of the measured stress results with the linear finite element and formula predictions are not as good as was expected. The measured meridional stress at the stiffener shell connection at failure was (from Table 1) 35,699 psi compared to 38,350 psi from the finite element results. The measured midbay stresses at failure were 27,515 psi in the circumferential direction and 13,974 psi in the meridional direction. The corresponding finite element results are 33,405 and 16,138 psi, respectively. The Salerno and Pulos formula for midbay circumferential stress gives 34,928 psi. The measured results seem to be on the low side, particularly at midbay. Some reasons for this may be:

- the actual model is on average slightly thicker than the 0.06 inch nominal thickness
- the gauges may be slightly out of line - it would be possible to calibrate the gauges on the structure only by comparing them to numerical results, which is the purpose of the test, so no calibration was done, and
- the shell is experiencing some geometric nonlinearities.

The first two reasons should only have small influences on the stresses. The third reason is possible, as the finite element results indicate a radial deflection of 0.009 inches between midbay and the ring stiffener at the failure pressure. This is 0.15 times the shell thickness, which is within the range where large deflection theory begins (0.1 to 0.2 times the shell thickness). Large deflections (geometric nonlinearities) would increase the stiffness and thus lower the strain gauge readings.

The fact that the meridional stress near the shell-stiffener intersection approaches the yield stress of 41,000 psi explains the catastrophic failure, and plentiful evidence of yielding is apparent in the collapsed model. The strain gauges cannot detect the peak stress in this area as they average over their width. The finite element model also averages over element widths. In fact, a local nodal stress value, before averaging, of 42,000 psi occurs in the finite element results at

the connection point. It is therefore quite likely that in the range of 590 psi pressure a local yield was attained at the shell-stiffener intersection, leading to collapse.

As mentioned, it was evident from the strain gauge data that there was sufficient energy in the tank to excite the model vibration modes. This appears to be a result of unsteady motion of the pump system producing shock waves in the tank. This allowed an investigation using model natural frequency data to predict buckling loads. The basic theory of using the frequency squared versus the applied pressure has been described in Section 2. This technique has been investigated extensively by Singer[2] for nondestructive evaluation of buckling loads including uncertainties in boundary conditions and initial imperfections. Most of his work was on axially loaded, stringer stiffened (stiffeners in meridian axis) cylinders. Singer used an electromagnetic shaker to excite the models and mode shapes were determined by scanning the shell with a microphone. Vibration frequencies for various modes were measured over a range of applied loading up to about 60 percent of the predicted classical buckling load. Straight lines were extrapolated through the frequency-squared points in the mode of failure to the point of zero frequency to determine the buckling load. Information from numerical calculations of the frequencies versus applied load was also used in producing the curves.

The main drawback in applying this method here was that there was insufficient instrumentation to identify mode shapes; only frequencies could be determined from the strain gauge data. Fourier spectra for five load levels were generated from the circumferential strain gauge data in bay 5, where collapse occurred. These spectra are shown in Figures 22 to 26. There are some fairly strong peaks in addition to the 60 Hz harmonics in these data. Some of the peaks also shift with increasing applied load. This can be more readily seen in Figure 27 which shows a cascade plot of frequency spectra versus load level. The predominant frequencies were squared and plotted against applied pressure in Figure 28. Broad peaks are plotted as bars to cover a range of frequencies. Finite element results for frequencies versus load were determined and straight lines of frequency-squared versus load were plotted on Figure 28 for the first eigenvalues of harmonics 0,1,2,7,8,9 and 10.

There are several things to note from Figures 22 to 28. There are frequency values of 544 Hz and approximately 470 Hz that remain constant throughout the loading history. The 544 Hz value may correspond to a finite element result of 530 Hz for the first eigenvalue of harmonic n=0 which is sometimes referred to as the 'breathing' mode. This finite element result remains at 530 Hz throughout the increase in loading. This frequency shows a significant amount of energy which is another characteristic of the breathing mode. The 470 Hz value probably corresponds to the finite element value of 418 Hz for the first eigenvalue of the n=1 harmonic which also remains constant with increased load. This is the fundamental beam bending mode of the model which should not change appreciably with increased pressure. It is also possible that this mode corresponds to the first eigenvalue of the n=2 harmonic for which the finite element analyses give values ranging from 500 Hz at 50 psi pressure to 462 Hz at 525 psi pressure. The lines on Figure 28 for harmonics n=0,1 and 2 pass through the experimental data fairly well.

The experimental data points on Figure 28 follow the general trend of the numerically derived lines for harmonics n=7,8,9 and 10. There are many modes which exhibit frequencies in this range. Figure 29 shows the first three eigenvalues for each of the first 10 harmonics at a load of 50 psi. Each point represents a mode and there would be more points if more than three modes per harmonic were determined. Therefore, it is difficult to ascertain which mode the experimental values correspond to. If we assume that the values correspond to the buckling modes, which are the first eigenvalues of each harmonic, identification is easier. This is a reasonable assumption as these modes should exhibit the most drastic decrease with increased load. Using Singer's method of extrapolating the data points from frequencies measured at loads less than 60% of the buckling load, a dashed line (Figure 28) is drawn through the points most likely to correspond to the n=9 harmonic in which buckling failure occurred. This gives a buckling failure load of 555 psi which is within the range of the actual value which lies between 540 and 587 psi.

A combination of the finite element analyses and limited modal data has resulted in a fairly successful prediction of the buckling load. It is planned to try this again for a model which buckles in an n=2 or n=3 overall mode and to identify the mode shapes with sufficient instrumentation. If successful, this could be useful in determining the overall buckling loads of full scale structures, such as submarine pressure hulls, by measuring vibrations at several locations on the circumference over the operating depth range of the pressure hull. Prior determination of the most likely buckling and frequency modes by a finite element program such as VAST would be a necessary part of the study to determine optimum positions for instrumentation and to evaluate the results.

Another aspect of vibration and stability analysis is that of parametric resonance. This occurs when a periodic forcing function drives certain vibration frequencies. The Mathieu[9] equation describes this behaviour where the loading function is a coefficient of the displacement in the equation of motion. For certain driving frequencies and amplitudes of the forcing function, the resultant vibration motion can be significantly amplified to the point of instability in the corresponding buckling mode. Periodic loading of amplitudes less than the static collapse load can cause failure in this manner. It is possible in this case that periodic loading from the pump system may have excited the n=9 mode near the failure point and caused the final pressure perturbation necessary for collapse.

7 Concluding Remarks

The experimental determination of the interframe buckling load of a ring stiffened cylinder served several purposes. The finite element code VAST successfully predicted the buckling load and mode, and also some of the predominant vibration frequencies. The fact that the predicted buckling load for the perfect model was very close to the actual buckling load is largely due to the excellent machining of the model by the Ship Repair Unit (Atlantic) which resulted in minimal imperfections in the model. More extensive measurement of the initial geometry would have been desirable to detect imperfections in the higher order modes where buckling occurred.

The pressure tank facility was shown to be suitable for model buckling tests although the inability to see the model during the test or monitor general displacements in some manner made determination of the exact buckling load difficult. The comparison of measured and predicted strain data was not as good as might be expected, but was still reasonable. The measured data showed the expected stress distribution.

The investigation of the decreasing frequency method for nondestructively determining buckling loads showed considerable promise, and will benefit from further work in this direction. More effort in measuring vibration mode shapes as opposed to just the frequency values should make this a viable technique to employ on full scale structures such as operational submarines. Determination of modes in shell structures which have many modes in the same frequency range will prove difficult, and it is unlikely that the interframe modes of a full scale structure could be definitively measured; however, overall buckling and vibration modes with circumferential harmonics of n=2 or n=3 may be discernable.

TIME (SEC)	SIGE8 (PSI)	SIGC5 (PSI)	SIGM5 (PSI)	PRESSURE (PSI)	
75.8180	-32294.08	-26382.28	-13208.72	545.8	
75.9850	-31525.17	-25613.38	-12954.98	543.3	
76.1520	-32403.92	-26378.99	-14088.57	536.0	SIGE8:
76.3190	-31635.01	-25869.31	-13137.32	545.8	MERIDIANAL STRESS
76.4860	-31635.01	-25942.91	-13063.72	543.3	AT SHELL-STIFFENER
76.6530	-32294.08	-25721.02	-13577.79	536.0	CONNECTION IN BAY 8
76.8200	-31415.33	-26236.19	-13062.62	543.3	
76.9870	-31744.86	-25759.47	-13101.07	545.8	SIGC5:
77.1540	-32184.23	-26013.21	-13869.98	528.7	CIRCUMFERENTIAL
77.3210	-31635.01	-26126.35	-13026.38	545.8	STRESS IN BAY 5
77.4880	-31964.55	-25685.87	-13174.67	543.3	
77.6550	-32623.61	-27040.25	-13719.49	545.8	SIGM5:
77.8220	-32513.76	-28649.46	-14739.94	545.8	MERIDIANAL
77.9890	-32403.92	-28466.02	-14777.29	548.2	STRESS IN BAY 5
78.1560	-32184.23	-26381.19	-13502.00	550.6	
78.3230	-31964.55	-25906.66	-12953.88	545.8	
78.4900	-32294.08	-26125.25	-13319.66	543.3	
78.6570	-32623.61	-26271.34	-13465.75	550.6	
78.8240	-31964.55	-25942.91	-13063.72	553.1	
78.9910	-32403.92	-26271.34	-13465.75	545.8	
79.1580	-33172.83	-26599.77	-13867.78	548.2	
79.3250	-32623.61	-26748.06	-13427.31	560.4	
79.4920	-32513.76	-26454.78	-13428.40	558.0	
79.6590	-32623.61	-26637.12	-13684.34	545.8	
79.8260	-33172.83	-26820.56	-13646.99	562.8	
79.9930	-32733.45	-26308.69	-13282.31	565.3	
80.1600	-32953.14	-26637.12	-13684.34	548.2	
80.3270	-33612.20	-27404.93	-14231.36	562.8	
80.4940	-32733.45	-26748.06	-13427.31	567.7	
80.6610	-33062.98	-26857.91	-13463.55	565.3	
80.8280	-33172.83	-26784.31	-13537.15	565.3	
80.9950	-33502.36	-26673.37	-13794.18	555.5	
81.1620	-33722.05	-27111.65	-14232.46	558.0	
81.3290	-34490.95	-27221.49	-14268.71	567.7	
81.4960	-33941.73	-27258.84	-14085.27	570.2	
81.6630	-34490.95	-27442.28	-14047.92	579.9	
81.8300	-34490.95	-27368.68	-14121.52	575.0	
81.9970	-34600.80	-27185.24	-14158.87	577.5	
82.1640	-34600.80	-27185.24	-14158.87	575.0	
82.3310	-34381.11	-26929.31	-13976.53	560.4	
82.4980	-34490.95	-26895.25	-13280.12	560.4	
82.6650	-34710.64	-27004.00	-13609.65	579.9	
82.8320	-34271.27	-27187.44	-13572.30	579.9	
82.9990	-34381.11	-26895.25	-13280.12	587.2	
83.1660	-34710.64	-26821.66	-13353.71	589.7	
83.3330	-34820.48	-27590.57	-13607.45	587.2	FAILURE
83.5000	-35699.23	-27515.87	-13974.33	589.7	
83.6670	-35259.86	-26637.12	-13684.34	579.9	
83.8340	-15817.51	-23255.03	-16189.88	506.7	
84.0010	111601.30	21225.12	-97631.37	6.5	
84.1680	98639.73	43713.44	-92069.98	50.4	

TABLE 1: Strain and Pressure Data Near Failure Point

TIME (SEC)	SIGC3 (PSI)	SIGM3 (PSI)	SIGC4O (PSI)	SIGC4I (PSI)	PRESSURE (PSI)	
0.0000	-16868.71	-8405.25	-16758.87	-17308.09	350.6	
0.1670	-17565.12	-8439.30	-17125.75	-16686.37	350.6	
0.3340	-17305.89	-9136.81	-18074.80	-17525.58	353.0	
0.5010	-17306.99	-8843.52	-17197.15	-17306.99	340.8	SIGC3:
0.6680	-16978.56	-8441.50	-17088.40	-16868.71	338.4	CIRCUMFERENTIAL
0.8350	-17052.15	-8367.90	-16942.31	-16942.31	360.3	STRESS IN BAY 3
1.0020	-17565.12	-8439.30	-17015.90	-16796.22	350.6	
1.1690	-17086.20	-9064.31	-17635.42	-17745.27	348.1	SIGM3:
1.3360	-16978.56	-8441.50	-17417.93	-16978.56	340.8	MERIDIANAL
1.5030	-17014.80	-8551.34	-17124.65	-17014.80	345.7	STRESS IN BAY 3
1.6700	-17162.00	-8404.15	-16832.46	-17162.00	350.6	
1.8370	-17196.05	-9100.56	-17305.89	-18184.64	345.7	SIGC4O:
2.0040	-17124.65	-8587.59	-17124.65	-17234.49	345.7	CIRCUMFERENTIAL
2.1710	-16978.56	-8441.50	-17088.40	-16649.02	350.6	STRESS IN OUTER
2.3380	-17380.58	-8769.93	-17819.96	-16941.21	353.0	FIBER IN BAY 4
2.5050	-17270.74	-8733.68	-17270.74	-17270.74	340.8	
2.6720	-16722.62	-8259.16	-17271.84	-16832.46	350.6	SIGC4I:
2.8390	-17199.34	-8220.71	-17309.19	-16869.81	353.0	CIRCUMFERENTIAL
3.0060	-16649.02	-8332.75	-16978.56	-17198.24	331.0	STRESS IN INNER
3.1730	-16942.31	-8331.65	-16832.46	-16502.93	355.4	FIBER IN BAY 4
3.3400	-17122.45	-9174.15	-17671.67	-17561.83	353.0	
3.5070	-16795.12	-8478.84	-17014.80	-17234.49	348.1	
3.6740	-17601.37	-8549.14	-17381.68	-16722.62	348.1	
3.8410	-17123.55	-8880.87	-17233.39	-17782.61	340.8	
4.0080	-16539.18	-8296.50	-16868.71	-17088.40	343.2	
4.1750	-17673.87	-8768.83	-17673.87	-16904.96	355.4	
4.3420	-16904.96	-8515.09	-17014.80	-16904.96	335.9	
4.5090	-16942.31	-8331.65	-17052.15	-16832.46	353.0	
4.6760	-17453.08	-8989.62	-18002.30	-17233.39	345.7	
4.8430	-17014.80	-8551.34	-16904.96	-17454.18	338.4	
5.0100	-16612.78	-8222.91	-17052.15	-17162.00	355.4	
5.1770	-17159.80	-8990.71	-18148.39	-17599.17	355.4	
5.3440	-16795.12	-8478.84	-17014.80	-17124.65	343.2	
5.5110	-16978.56	-8441.50	-16978.56	-16978.56	355.4	
5.6780	-17269.64	-9026.96	-17709.02	-17379.49	355.4	
5.8450	-16758.87	-8369.00	-16978.56	-17088.40	343.2	
6.0120	-17271.84	-8440.40	-16832.46	-17052.15	355.4	
6.1790	-17378.39	-9356.49	-17707.92	-18037.45	348.1	
6.3460	-16758.87	-8369.00	-17088.40	-17308.09	348.1	
6.5130	-17052.15	-8367.90	-16942.31	-16832.46	355.4	
6.6800	-17086.20	-9064.31	-17525.58	-17855.11	348.1	
6.8470	-16795.12	-8478.84	-17124.65	-17344.34	345.7	
7.0140	-17455.28	-8403.05	-16906.06	-17015.90	350.6	
7.1810	-17014.80	-8551.34	-17124.65	-17564.02	335.9	
7.3480	-17271.84	-8440.40	-16832.46	-16942.31	348.1	
7.5150	-16903.86	-8808.37	-17123.55	-17672.77	335.9	
7.6820	-16758.87	-8369.00	-16978.56	-16758.87	345.7	
7.8490	-17232.30	-9210.40	-17891.36	-17891.36	355.4	

TABLE 2: Strain and Pressure Data Near 350 psi

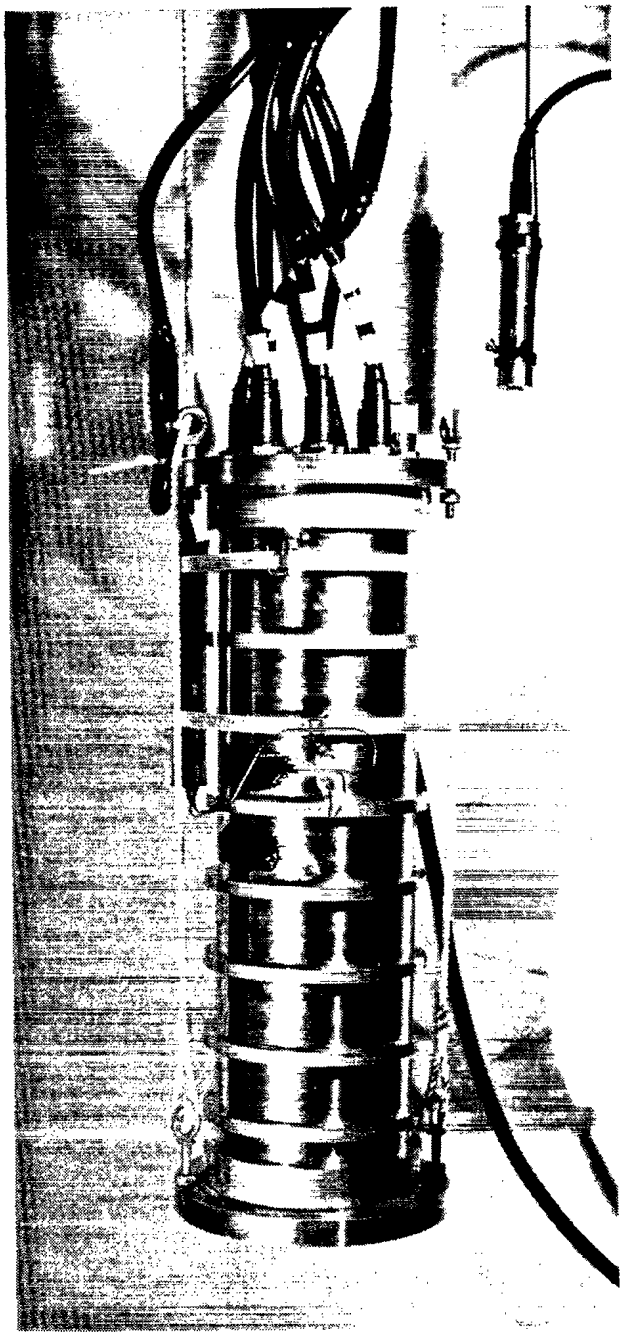

Figure 1: Photograph of Model Ring Stiffened Pressure Vessel

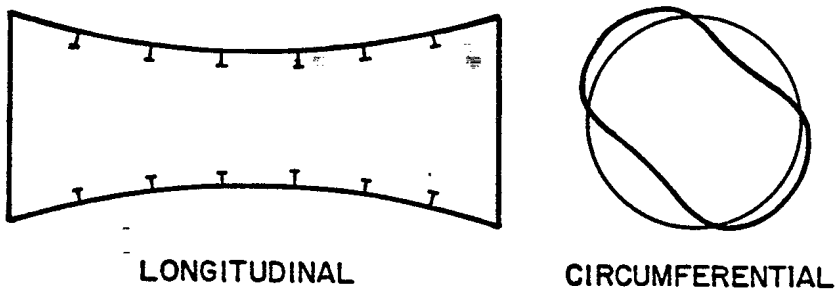

Figure 2: Overall Buckling Mode for A Ring Stiffened Cylinder

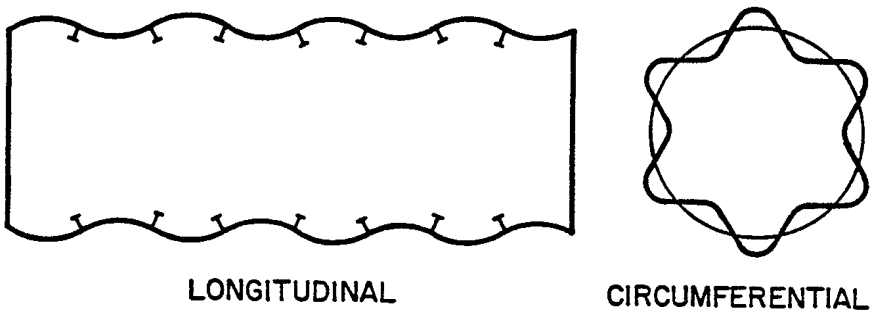

Figure 3: Interframe Buckling Mode for A Ring Stiffened Cylinder

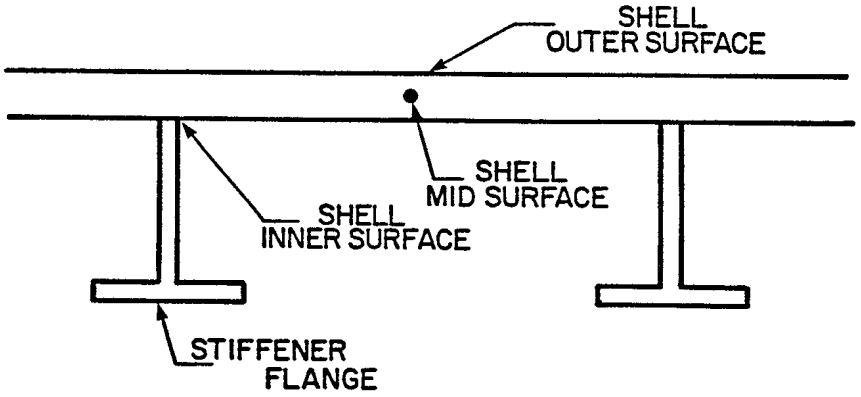

Figure 4: Critical Stress Locations for A Ring Stiffened Pressure Vessel

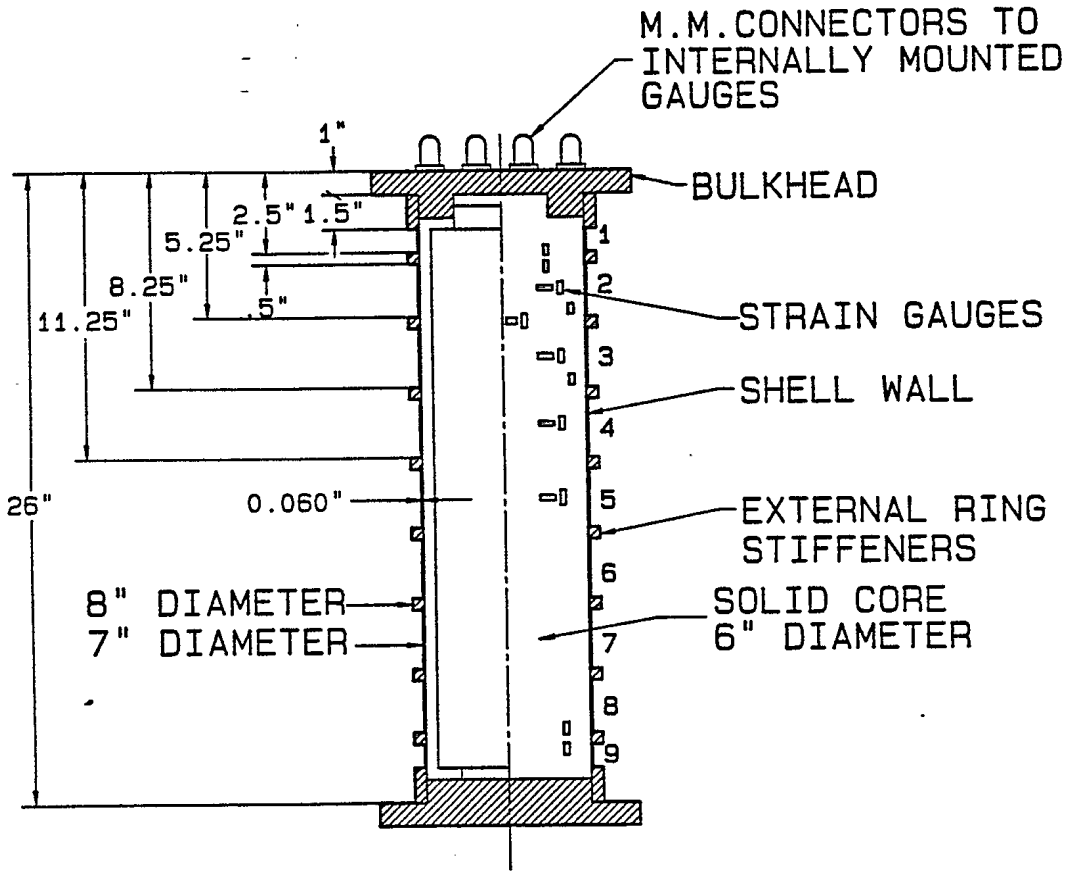

Figure 5: Schematic of Model Ring Stiffened Cylinder

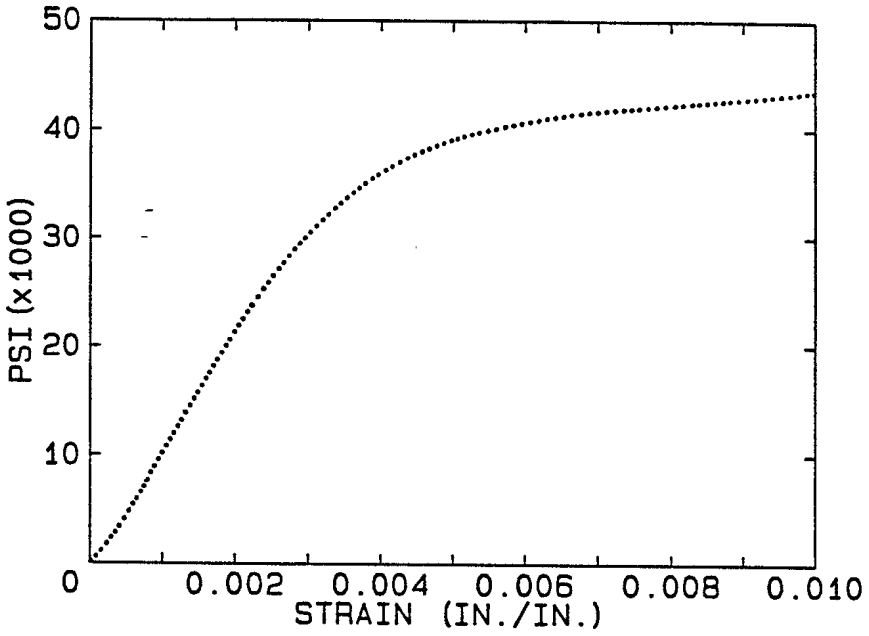

Figure 6: Measured Stress-Strain Curve for Model Material

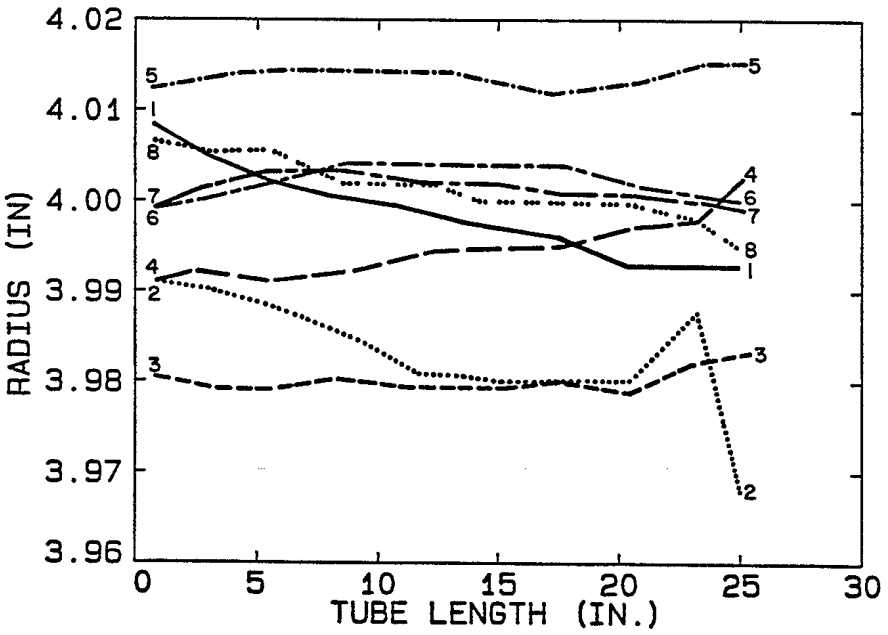

Figure 7: Radii to Outer Ring Surfaces over Length and Circumference

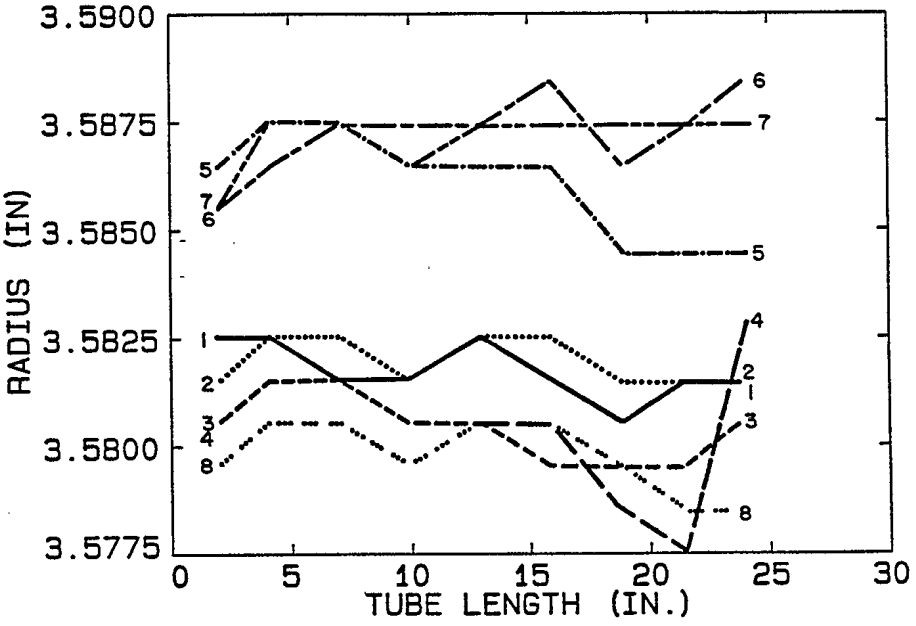

Figure 8: Radii to Outer Shell Surface over Length and Circumference

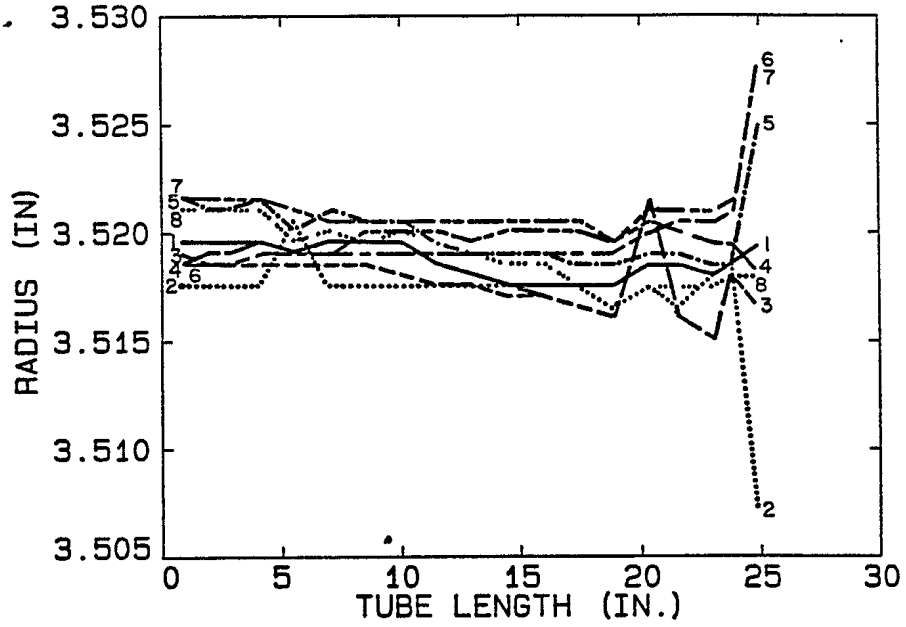

Figure 9: Radii to Inner Shell Surface over Length and Circumference

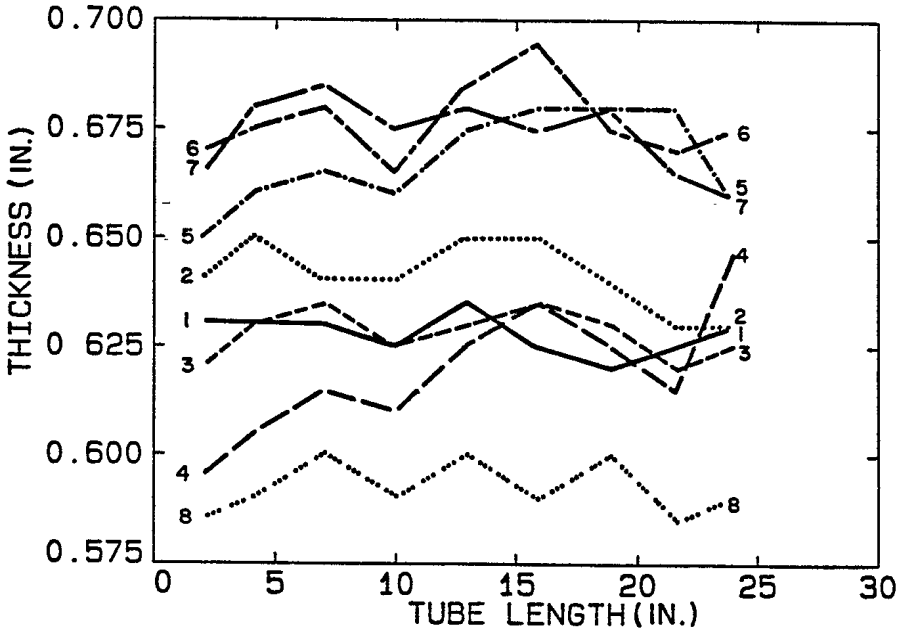

Figure 10: Shell Thickness over Length and Circumference

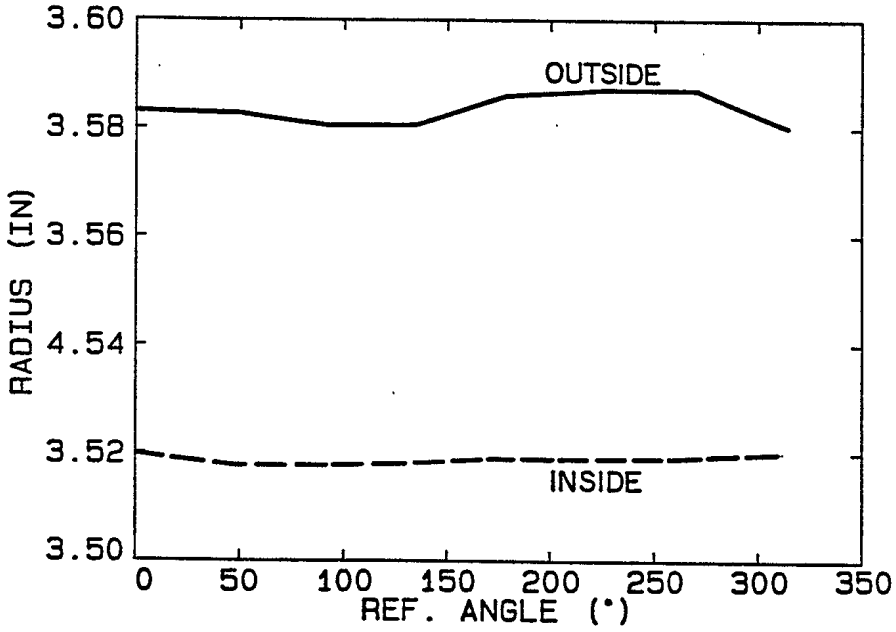

Figure 11: Radii of Shell Wall for Axial Location 13 Inches over Circumference

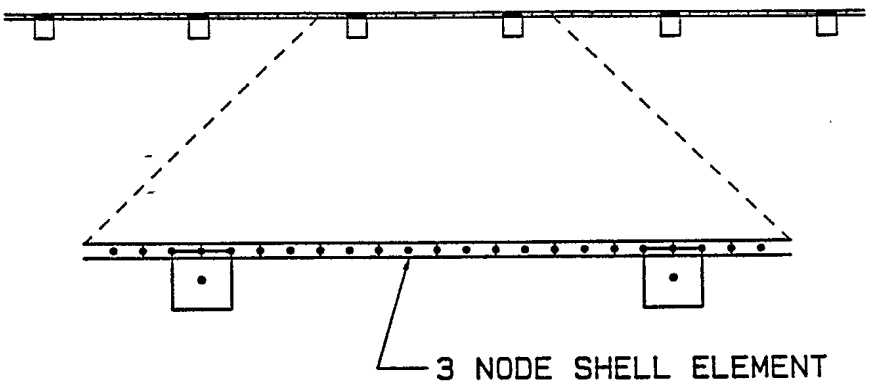

Figure 12: Axisymmetric Finite Element Model of Ring Stiffened Pressure Vessel

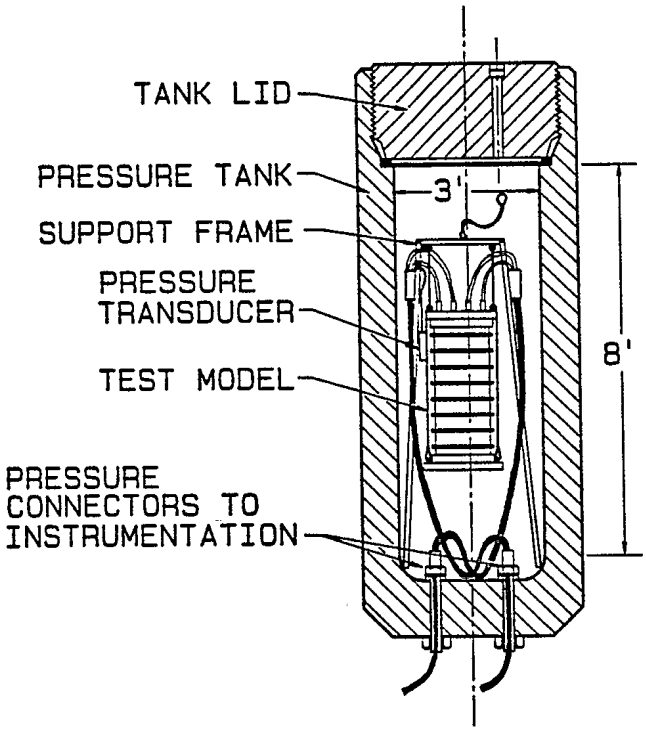

Figure 13: Schematic of Pressure Tank Facility and Test Setup

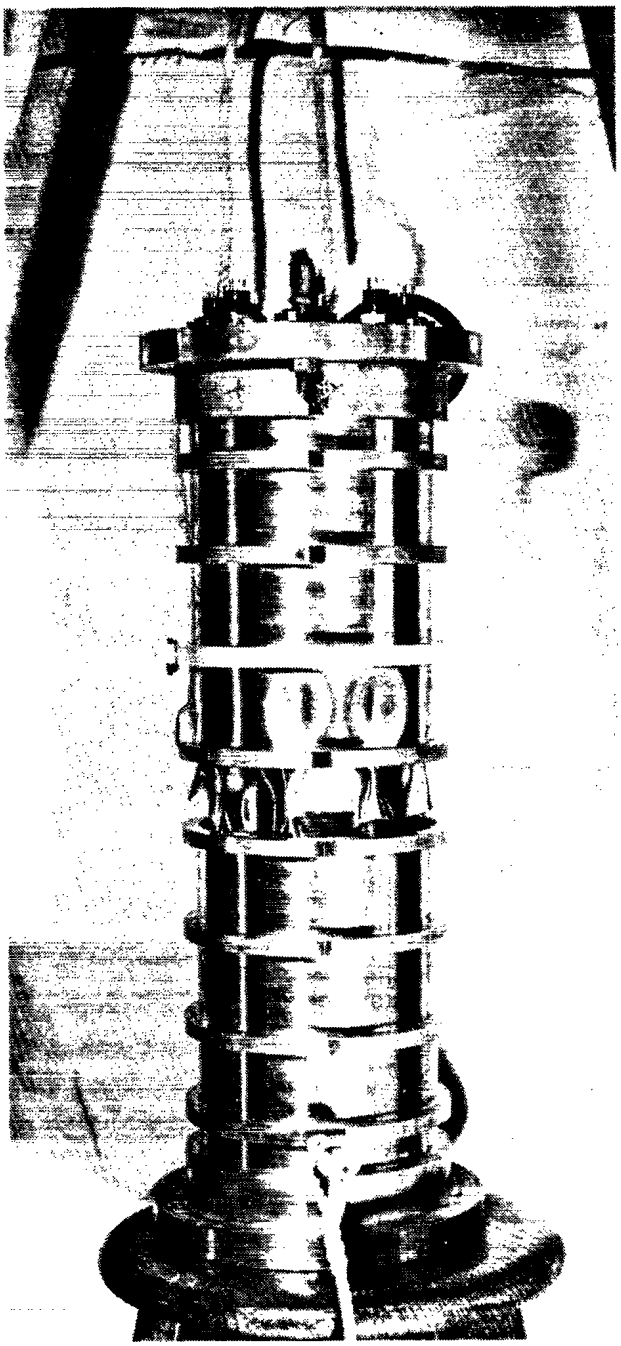

Figure 14: Collapsed Model

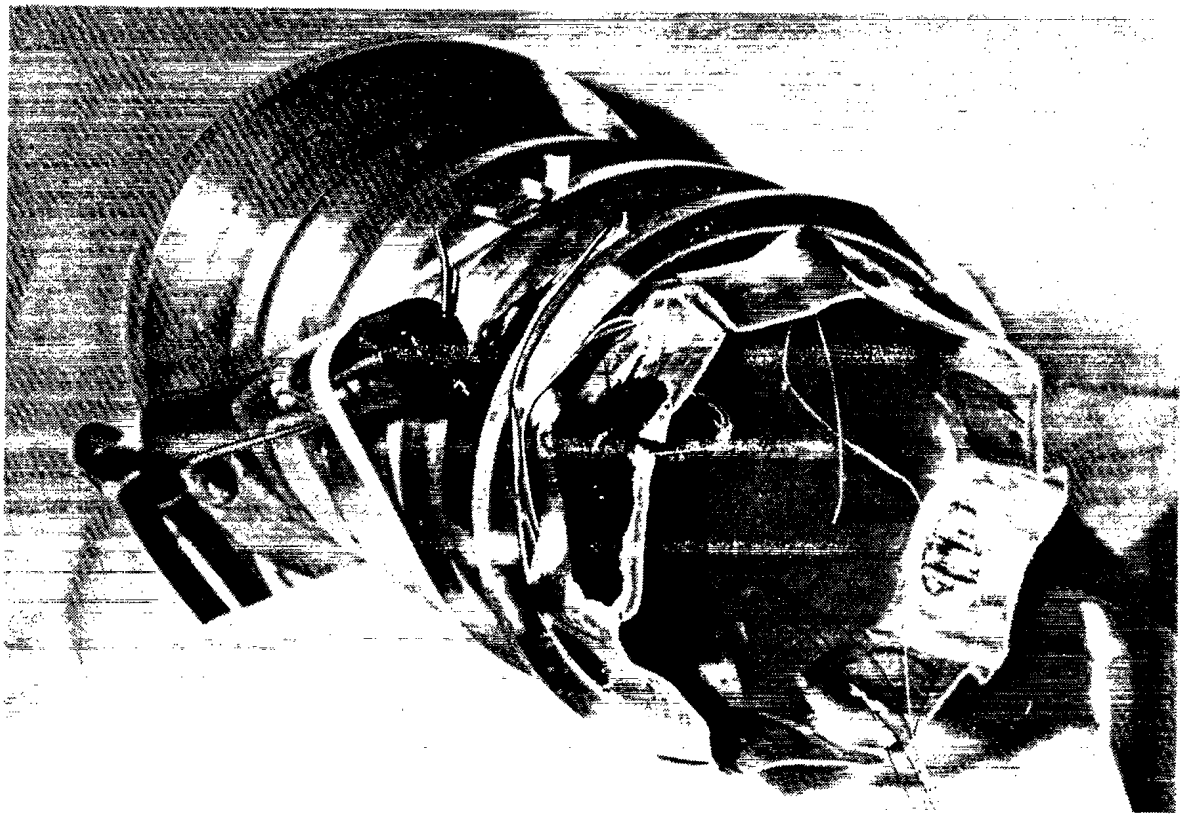

Figure 15: Collapsed Model Cross-Section

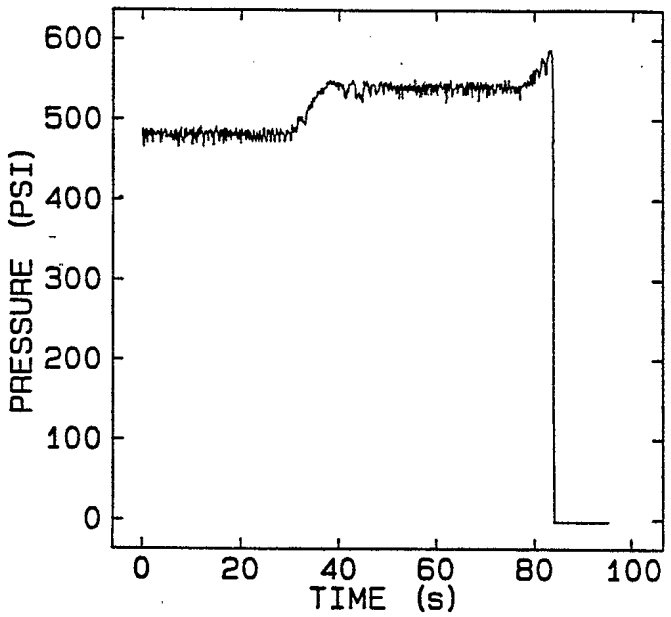

Figure 16: Pressure Time History in Region of Failure

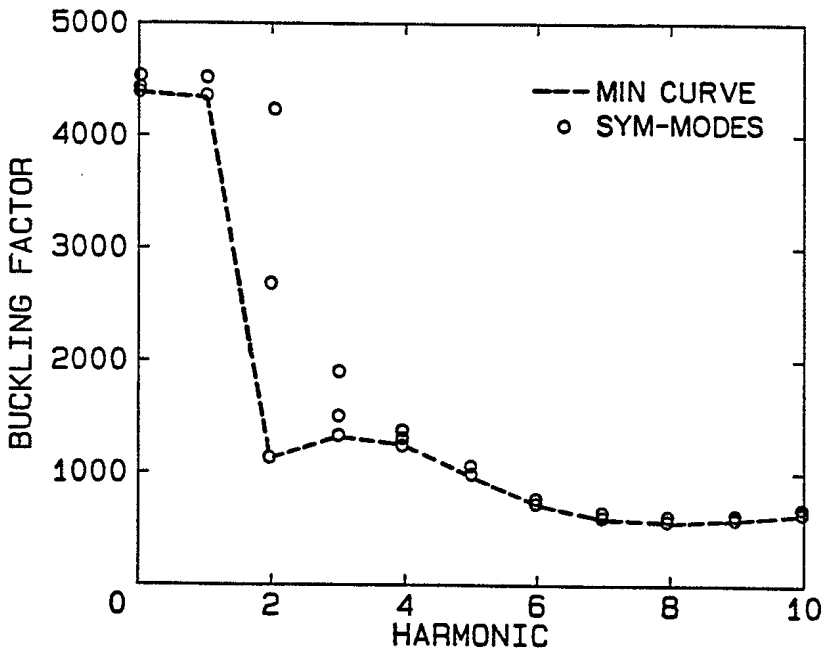

Figure 17: Buckling Load versus Circumferential Harmonic from Finite Element Results

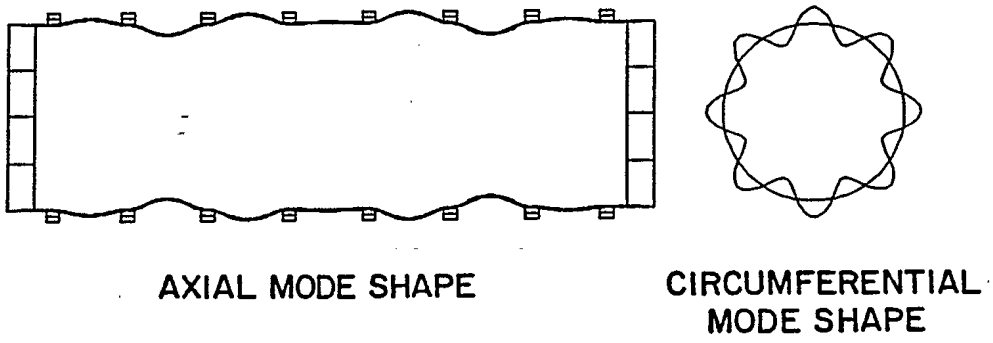

Figure 18: Buckling Mode in Harmonic n=8 from Finite Element Analysis, P_{cr}=568 psi

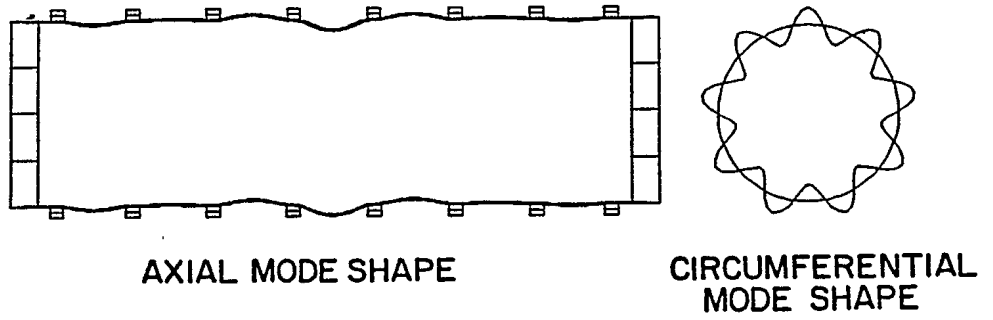

Figure 19: Buckling Mode in Harmonic n=9 from Finite Element Analysis, P_{cr}=588 psi

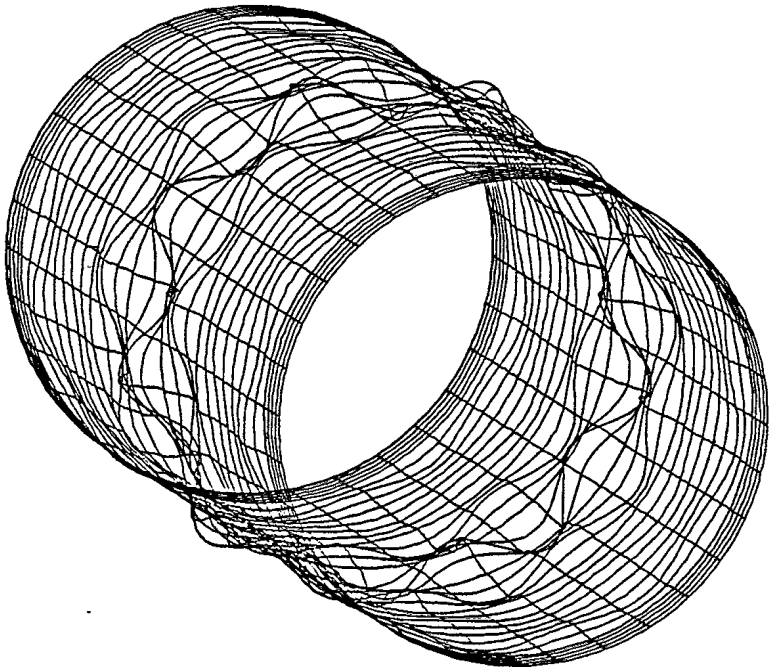

Figure 20: Three Dimensional Expansion of n=9 Buckling Mode from Finite Element Analysis

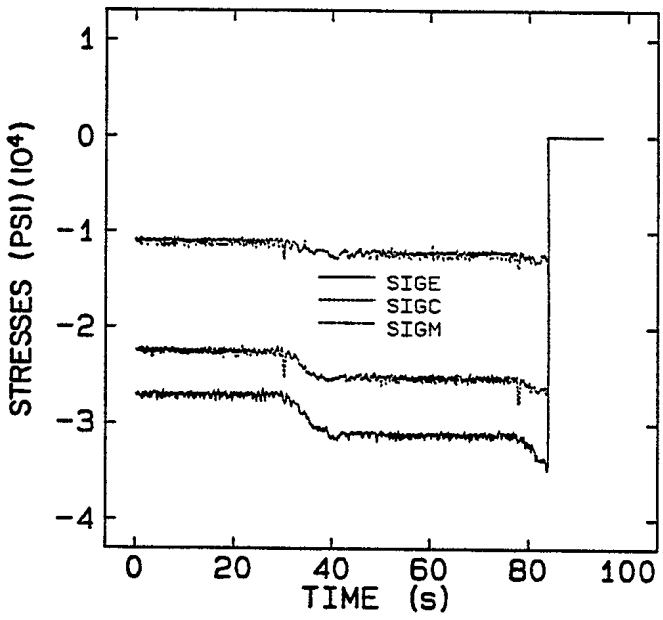

Figure 21: Stress Data in Region of Failure

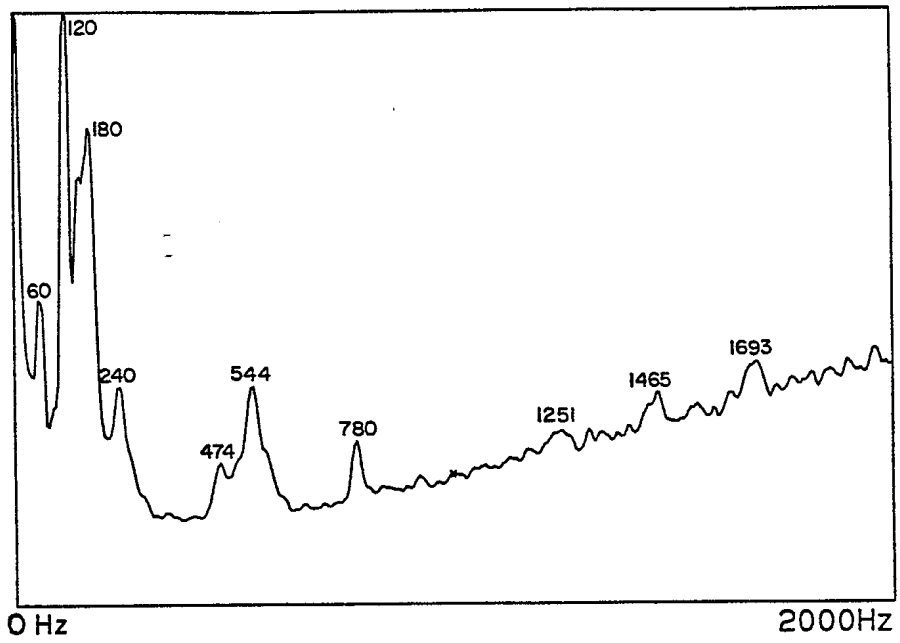

Figure 22: Fourier Spectra from Gauge in Failed Bay at 50 psi Pressure

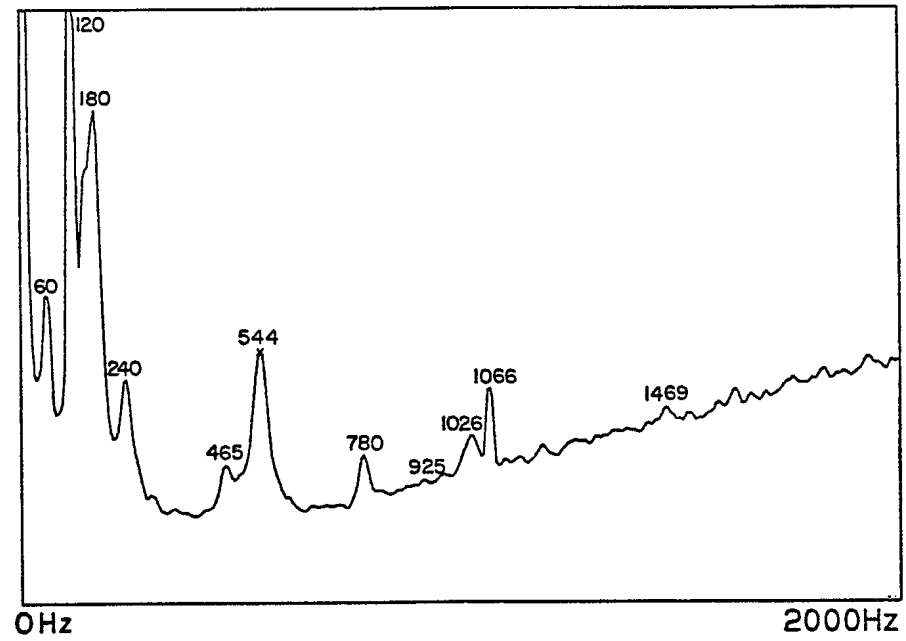

Figure 23: Fourier Spectra from Gauge in Failed Bay at 275 psi Pressure

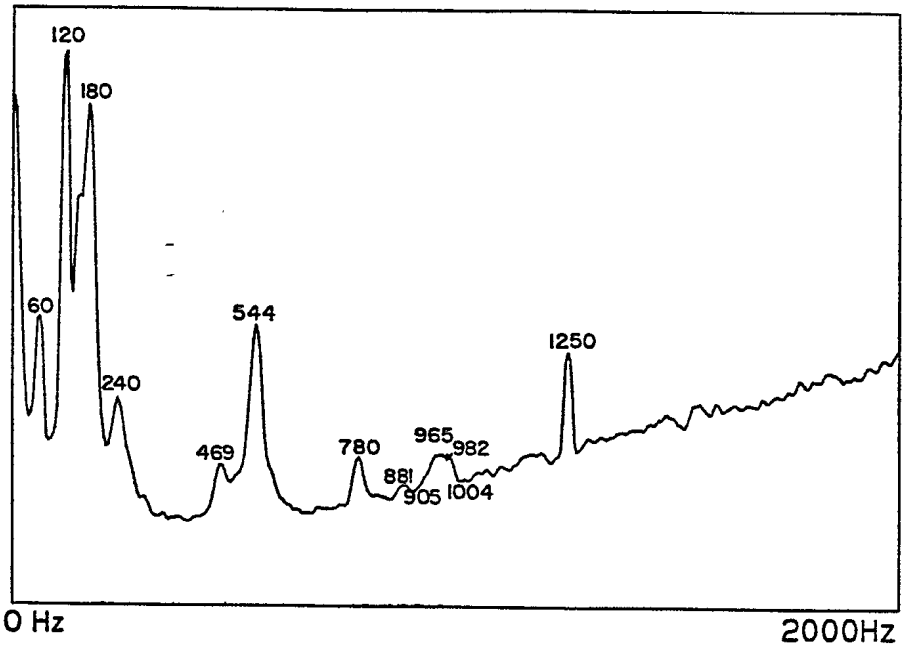

Figure 24: Fourier Spectra from Gauge in Failed Bay at 325 psi Pressure

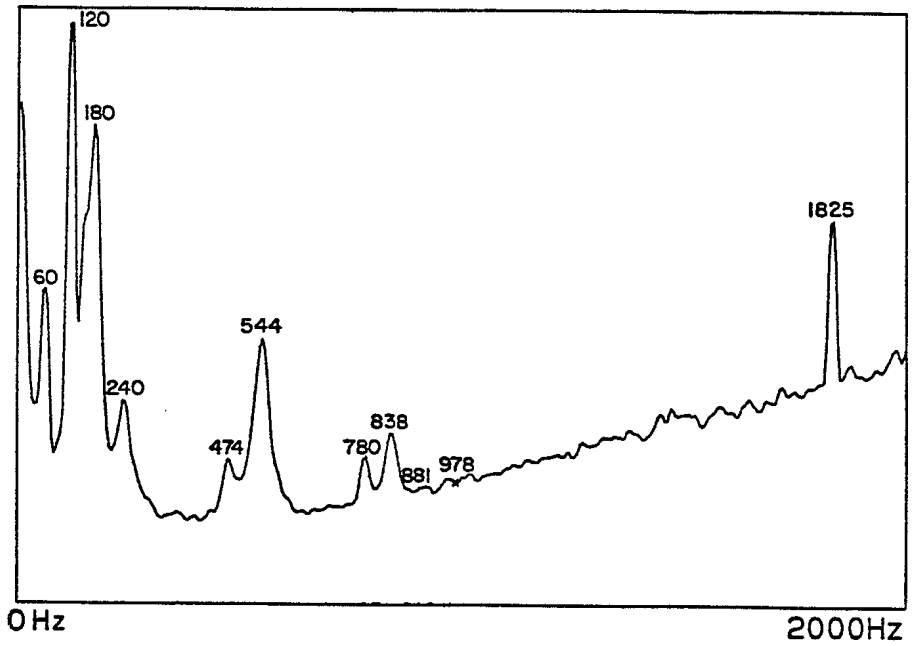

Figure 25: Fourier Spectra from Gauge in Failed Bay at 475 psi Pressure

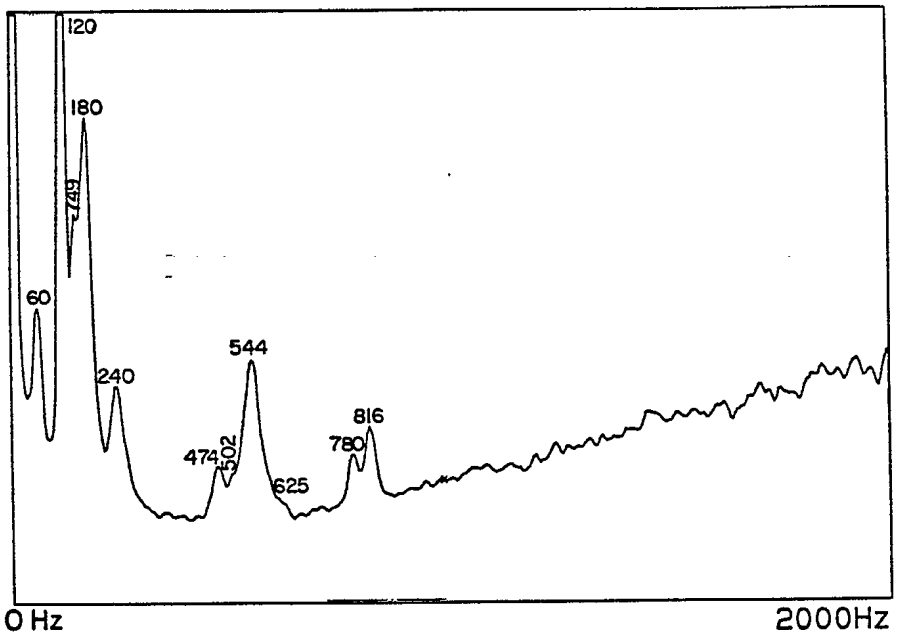

Figure 26: Fourier Spectra from Gauge in Failed Bay at 525 psi Pressure

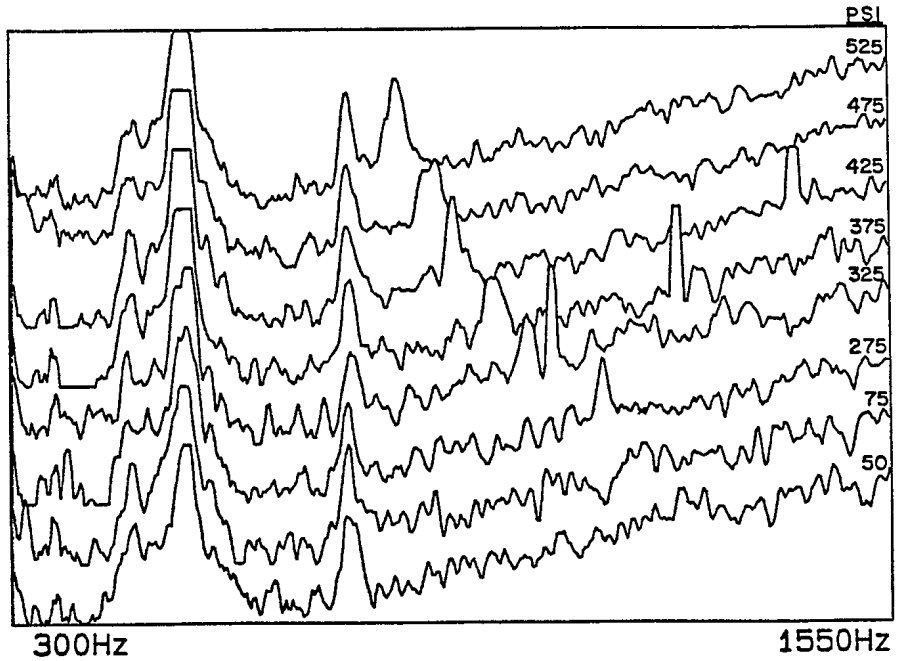

Figure 27: Cascade Fourier Spectra from Gauge in Failed Bay for Pressures Ranging from 50 psi to 525 psi

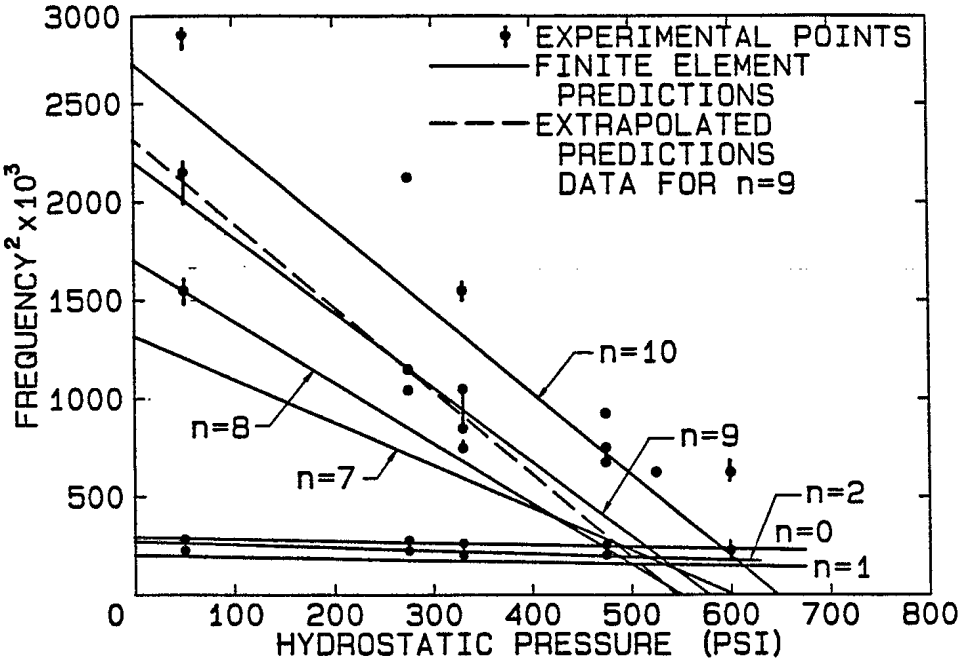

Figure 28: Frequency-Squared versus Applied Pressure from Gauge in Failed Bay and Results of Finite Element Analyses

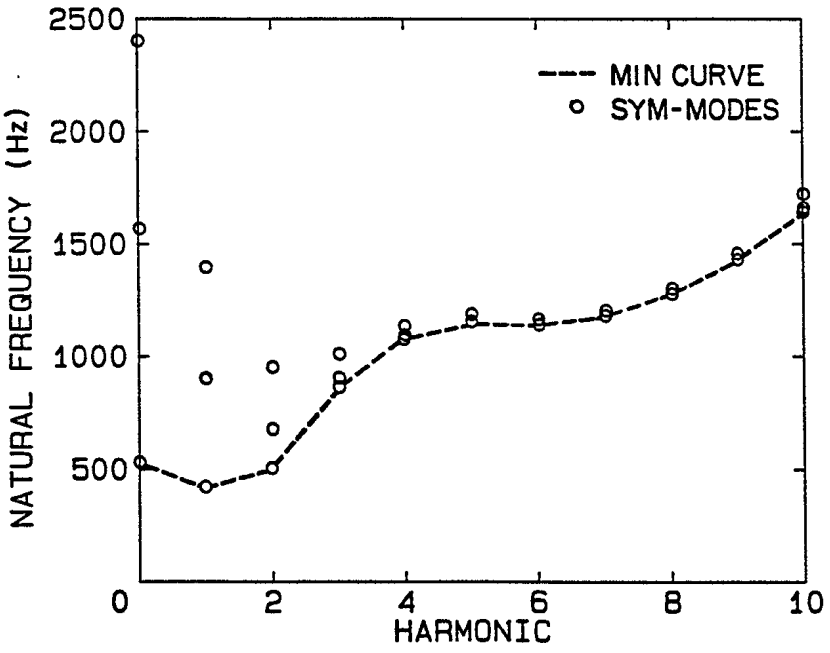

Figure 29: Natural Frequency versus Circumferential Harmonic from Finite Element Results

References

1. 'Vibration and Strength Analysis Program (VAST), Version 04', Martec Ltd, Halifax, Nova Scotia, DREA Contract Report CR 86/429, Dartmouth, N.S., 1986.

2. Singer J.,'Vibrations and Buckling of Imperfect Stiffened Shells - Recent Developments', in 'Collapse: The Buckling of Structures in Theory and Practice', ed. J.M.T. Thompson and G.W. Hunt, Cambridge University Press, London, 1983.

3. Seleim S.S., Roorda J.,'Buckling Behaviour of Ring Stiffened Cylinders: Experimental Study', Thin-Walled Structures, Vol 4, No 3, 1986.

4. British Standard Specification for Unfired Fusion Welded Pressure Vessels, British Standard Institution BS5500, Issue 5, April 1980.

5. Kendrick S., 'The Buckling Under External Pressure of Ring Stiffened Circular Cylinders', RINA Trans, Vol 107, 1965.

6. Gill S.S., The Stress Analysis of Pressure Vessels and Pressure Vessel Components, Pergamon Press, Toronto, 1970.

7. Pegg N.G., Smith D.R., ' PRHDEF - Stress and Stability Analysis of Ring Stiffened Submarine Pressure Hulls', Defence Research Establishment Atlantic Technical Memorandum 87/213, June, 1987.

8. Nigh G.L., DesRochers C.G., 'Stress and Buckling of Reinforced Shells', Martec Ltd, Final Report, DREA Contract 10SC.97707-3-3737, Sept, 1985.

9. Bolotin V.V, The Dynamic Stability of Elastic Systems, Holden-Day Inc., London, 1964.

DOCUMENT CONTROL DATA

(Security classification of title, body of abstract and indexing annotation must be entered when the overall document is classified)

1. ORIGINATOR (the name and address of the organization preparing the document. Organizations for whom the document was prepared, e.g. Establishment sponsoring a contractor's report, or tasking agency, are entered in section 8.)

Defence Research Establishment Atlantic

2. SECURITY CLASSIFICATION (overall security classification of the document, including special warning terms if applicable)

Unclassified

3 TITLE (the complete document title as indicated on the title page. Its classification should be indicated by the appropriate abbreviation (S,C,R or U) in parentheses after the title.)

Experimental Determination of Interframe Buckling of a Ring Stiffened Cylinder.

4. AUTHORS (Last name, first name, middle initial. If military, show rank, e.g. Doe, Maj. John E.)

Pegg, Neil G.

5. DATE OF PUBLICATION (month and year of publication of document)	6a. NO. OF PAGES (total containing information. Include Annexes, Appendices, etc.)	6b. NO. OF REFS (total cited in document)
May 1989	38	9

6. DESCRIPTIVE NOTES (the category of the document, e.g. technical report, technical note or memorandum. If appropriate, enter the type of report, e.g. interim, progress, summary, annual or final. Give the inclusive dates when a specific reporting period is covered.)

Technical Memorandum

8. SPONSORING ACTIVITY (the name of the department project office or laboratory sponsoring the research and development. Include the address.)

9a. PROJECT OR GRANT NO. (if appropriate, the applicable research and development project or grant number under which the document was written. Please specify whether project or grant)	9b. CONTRACT NO. (if appropriate, the applicable number under which the document was written)
1AE	

10a. ORIGINATOR 'S DOCUMENT NUMBER (the official document number by which the document is identified by the originating activity. This number must be uniqué to this document.)	10b. OTHER DOCUMENT NOS. (any other numbers which may be assigned this document either by the originator or by the sponsor)
DREA Technical Memorandum 89/209	

11. DOCUMENT AVAILABILITY (any limitations on further dissemination of the document, other than those imposed by security classification)

(X) Unlimited distribution
( ) Distribution limited to defence departments and defence contractors; further distribution only as approved
( ) Distribution limited to defence departments and Canadian defence contractors; further distribution only as approved
( ) Distribution limited to government departments and agencies; further distribution only as approved
( ) Distribution limited to defence departments; further distribution only as approved
( ) Other (please specify):

12.. DOCUMENT ANNOUNCEMENT (any limitations to the bibliographic announcement of this document. This will normally correspond to the Document Availability (11). However, where futher distribution (beyond the audience specified in 11) is possible, a wider announcement audience may be selected.)

13. ABSTRACT (a brief and factual summary of the document. It may also appear elsewhere in the body of the document itself. It is highly desirable that the abstract of classified documents be unclassified. Each paragraph of the abstract shall begin with an indication of the security classification of the information in the paragraph (unless the document itself is unclassified) represented as (S), (C), (R), or (U). It is not necessary to include here abstracts in both offical languages unless the text is bilingual).

An experimental determination of the interframe buckling collapse of a ring stiffened cylinder subjected to hydrostatic pressure is presented. This test served two purposes; the first to experimentally verify finite element predictions of the buckling collapse behaviour, the second to evaluate the possibilities of using an existing high pressure facility for conducting model tests of more complex pressure vessel models. The finite element and experimental results for the collapse load and mode were in good agreement. A method of determining the elastic buckling collapse load by measuring the decreasing frequencies of vibration modes corresponding to buckling collapse modes has also been investigated with encouraging results. The high pressure tank served the purpose of conducting the experiment, although the inability to physically observe the test did cause some difficulties in determining the actual collapse load.

14. KEYWORDS, DESCRIPTORS or IDENTIFIERS (technically meaningful terms or short phrases that characterize a document and could be helpful in cataloguing the document. They should be selected so that no security classification is required. Identifiers, such as equipment model designation, trade name, military project code name, geographic location may also be included. If possible keywords should be selected from a published thesaurus. e.g. Thesaurus of Engineering and Scientific Terms (TEST) and that thesaurus-identified. If it is not possible to select indexing terms which are Unclassified, the classification of each should be indicated as with the title.)

Buckling
Structural stability
Experimental
Cylinder
Ring-Stiffened
Submarine

84-02819
60722